

Data Reduction Considerations for the Burning Velocity of Spherical Constant Volume Flames of R32 (CH₂F₂) with Air

Michael J. Hegetschweiler ^a, Lukas Berger ^b, Raik Hesse ^b, Joachim Beeckmann ^b, Chaimae Bariki ^b,
Heinz Pitsch ^b, Gregory T. Linteris ^{a,*}

^a National Institute of Standards and Technology, Gaithersburg, USA

^b Institute of Combustion Technology, RWTH Aachen University, Aachen, Germany

Combustion and Flame, Volume 254, August 2023, 112807

* corresponding author, linteris@nist.gov 301-975-2283

Data Reduction Considerations for the Burning Velocity of Spherical Constant Volume Flames of R32 (CH₂F₂) with Air¹

Michael J. Hegetschweiler ^{a,*}, Lukas Berger ^b, Raik Hesse ^b, Joachim Beeckmann ^b, Chaimae Bariki ^b, Heinz Pitsch ^b, Gregory T. Linteris ^a

Abstract

The present work explores data reduction techniques for the measurement of the laminar burning velocities of R32(CH₂F₂)-air mixtures using a constant volume combustion device, in which the pressure-time history is the only measured parameter. To allow clear assessment of the accuracy of the data reduction methods, the pressure-time histories used for analysis are synthetically generated via a detailed numerical simulation employing full kinetics and with and without an optically-thin radiation model. Various data reduction models are employed, including a two-zone model and two multi-zone models, and these are compared with the results from the burning velocity obtained from the output of the numerical simulation. The data reduction schemes are shown to be accurate if the same radiation model is employed in the data reduction as was used in the flame simulation to generate the pressure trace used for post-processing. If the incorrect radiation model is employed, however, the errors can be quite large. The effects of stretch, radiation, and different data post-processing methodologies are explored and the errors quantified. Stretch is shown to be important for the early stages and the selected data range that is used for extrapolation has a significant effect on the extrapolated burning velocity. However, with an appropriate choice of data considered for extrapolation, the prediction of the unstretched burning velocity can be quite accurate.

Keywords: Burning Velocity; Flame Stretch; Radiation; Laminar Flame Speed; Refrigerant Flammability; R32; difluoromethane; CH₂F₂.

1. Introduction and Background

Refrigerants for heat pumps, air-conditioning and refrigeration devices are widely used and typically have high global warming potential (GWP). Leakage from such devices as well as their improper disposal can lead to refrigerant escaping into the atmosphere and contributing to the greenhouse effect. For example, it has been estimated that hydrofluorocarbons (HFC) refrigerants will contribute about 20% of the total increase in radiative forcing between 2012 and 2050 [1]. New low-GWP compounds are being developed which have a higher reactivity such that they break down more quickly in the troposphere. Unfortunately, the higher reactivity makes them more flammable, a property which is an additional constraint for the Heating, Ventilation, Air Conditioning, and Refrigeration (HVAC&R) industry. A better fundamental understanding of their flammability will contribute to their safe use, and it is of value to develop modeling tools to rank their flammability and predict their behavior in various scenarios. The laminar burning velocity S_u of a flammable premixed gas mixture has been identified as an appropriate first target for predictive tools since it is a fundamental combustion parameter for a

¹ Official contribution of NIST, not subject to copyright in the United States. Certain commercial equipment, instruments, and materials are identified in this paper to adequately specify procedure. Such identification does not imply recommendation or endorsement by the National Institute of Standards and Technology.

mixture encompassing the effects of heat release, overall reaction rate, and transport. It correlates with the explosion pressure, venting requirements, turbulent flame propagation, minimum ignition energy, flame quenching distance, and extinction limits.

Experimental measurements of burning velocity are an indispensable ingredient for calibrating a model, with which predictions of the burning velocity at arbitrary conditions are then possible, and various arrangements have been used. For refrigerant flames, these include vertical tubes with quasi-1D planar flames [2-4], nozzle-burner Bunsen flames [5], and spherical outwardly propagating flames [6-15]. The latter, also known as spherically expanding flames (SEFs), can be conducted via the constant pressure method (CPM) or the constant volume method (CVM) method. In the first approach, also called an unconfined method, a spherical flame evolves in a quasi-isobaric environment and the flame is observed with an optical system. From the recorded images, the flame radius history $R_f(t)$ is extracted and the flame velocity deduced. In the CVM approach, the mixture is ignited in the confined environment of a constant volume chamber. The flame develops under the effect of increasing pressure and temperature due to the burned gas expansion. The flame advancement can be determined optically, with flame ionization detectors, or from the pressure rise. Advantages of the CPM are the conceptually simple data reduction (when radiation is not important), the possibility of deducing the stretch effects, and easily obtained data at ambient conditions. Disadvantages include a more expensive set-up due to the need for a schlieren or shadowgraph arrangement and high-speed camera, and the need to correct the raw data for contraction of the flame from thermal radiation from the burned gases [13, 15, 16], for example using the methods presented previously [14, 17]. Advantages of the CVM are the possibility of obtaining burning velocity data over a wide range of temperature and pressure from a single experiment, the possibility of simultaneous flame image and pressure rise data [18], and burning velocities from the pressure rise only. The last method is the subject of the present work. It has the advantages of a relatively simple experiment and small quantities of reactants and (toxic) products; disadvantages include the requirement of a thermodynamic model to relate the flame radius to the pressure rise, unquantified stretch effects on the flame speed at small radii, and unknown effects from the presence of flame instabilities (since flame images are not recorded). Also, if data are desired at ambient conditions, it is generally necessary to extrapolate the burning velocities from higher temperature T and pressure p back to ambient. Finally, heat loss via thermal radiation from the burned gases must be accounted for. The present work aims to explore the influence of stretch, thermal radiation, and extrapolation on the extracted laminar burning velocity from the post-processing of the pressure rise data. This is important to the HVAC industry since a simple method is needed for measuring the burning velocity of new, mildly flammable refrigerants to rank their flammability. Nonetheless, the measurements and data reduction for these compounds are challenging due to the toxic and corrosive products and the low burning velocities, for which buoyancy effects and thermal radiation from the product gases are more important as compared to hydrocarbon flames. Previous work on data reduction techniques for CVM are outlined below, followed by discussion of previous CVM work on refrigerant flames.

Seminal work on the CVM was described by Lewis and Elbe [19], Fiock and Marvin [20], Bradley and Mitcheson [21], in which the authors derived thermophysical models to calculate the flame velocities based on the measured time-pressure history. Subsequently, Metghalchi and Keck [22] developed a two-zone model which employs a simplified post-processing model and applied it to propane-air flames for a wide range of pressures and temperatures. Furthermore, they introduced a power-law correlation to describe the dependency of the flame velocity on the pressure and temperature of the unburned mixture. They compared it to the Arrhenius type correlation by Lavoie [23] and found that both perform similarly. In later work, Metghalchi and Keck [24], studying methanol, iso-octane, and indolene flames with air, extended their data reduction model to consider wall heat losses, thermal preheat zone ahead of the reaction zone, the energy input by a spark, heat losses to ignition electrodes, radiation of burned gas, and gradients in the burned gas. They concluded that most of these have negligible influence on the flame velocity and that the calibration of the pressure sensor is most important. Elia et al. [25] developed a multi-zone data reduction model, in which the burned gas is subdivided into multiple shells, allowing for non-uniform burned gas properties and the inclusion of more accurate radiation heat losses. They also considered stretch effects on the burning velocity, applying models of Bradley et al. [26] and

Aung et al. [27] to obtain stretch-free values for methane-air-diluted mixtures at a broad range of pressures and reactant temperatures.

The constant volume method has been used to measure the burning velocity of many refrigerants. Takizawa and co-workers have reported burning velocity data from CVM experiments for air with the refrigerants R32, R143, R143a, and R152a [6]; R41, R152, and R161 [7]; and R1234yf, R1234ze(E) [28], as well as from CPM experiments. Using the CVM, Takizawa et al. [6, 9] investigated fluorinated fuel compounds with the spherical flame setup and were among the first who applied the CVM and CPM methods to very slow-burning mixtures. They applied the CVM method with optical access and Schlieren system to R32, R143, R143a, and R152a flames [6] and concluded that the pressure-only CVM method works well for those compounds. In later work [9] flames of R32/Air and a fuel mixture of R32/R134a with air were measured with CVM under microgravity conditions and compared with CPM under normal gravity conditions. The S_u results from the two measurements agreed within $\pm 6\%$; however, the effect of radiation was not considered. Moghaddas et al. [29] used spherical and cylindrical vessels with optical access to obtain flame velocities of R32 and R152a by the CVM method. They applied an extended multi-zone model with different heat loss models to obtain flame velocities from the measured pressure trace. Furthermore, the stretch effects on the flame were investigated by initializing the experiment at different pressures and temperatures still on their relevant isentrope (450 K and 2.83 bar). No notable stretch dependency of R152a flame speeds between stretch rates 20 s^{-1} to 80 s^{-1} could be found.

Recently, extensive work has been done to understand the accuracy of the CVM. Omari et al. [30] used both CVM and CPM to obtain flame velocities of $\text{CH}_4/\text{H}_2/\text{air}$ mixtures. In the CPM method, they applied different zero stretch extrapolation correlations and corrected the results for radiation as suggested by Yu et al. [31]. To obtain the burned gas fraction-pressure relation in the CVM method, they applied analytical correlations to account for radiation heuristically. Faghieh and Chen [32] provided a review article on the CVM (with less emphasis on the CPM method). They showed that results of measured burning velocities vary considerably among different research groups, even for methane combustion, and they concluded that it is important to identify uncertainties and account for physical effects such as radiation. Employing the results of 1-D spherical numerical simulations, they also considered different available analytical correlations between burned gas mass fraction and pressure. Xiouris et al. [33] performed a thorough uncertainty quantification for the CVM experiment via a new multi-zone data reduction model, HTDR, which includes a radiation model. Three main uncertainty contributions were identified: mixture preparation, data acquisition, and data processing. They stressed the importance of including radiation and stretch effects in the data processing. An additional interesting and important finding is that comparing flame radius traces to evaluate the performance of a data reduction model is not sufficient since an error of 1.5% in the flame radius R_f can lead to an error of 15% in the flame velocity. Recently, Halter et al. [18] presented an advanced measurement technique to simultaneously measure pressure and flame radius up to the chamber walls using the CVM method. They showed that the evaluation of the flame radius is a major source of error, which can only be improved with very accurate measurement. Movaghar et al. [19], considering C_1 to C_4 hydrocarbons under engine-relevant conditions (8 bar to 30 bar and 400 K to 520 K) in a CVM experiment, assessed the uncertainties in the CVM method and studied which simplifications are appropriate. They found that an accurate evaluation of the flame radius is critical and the assumption of chemical equilibrium in the burned gas is justified; however, radiation and product dissociation must be considered. Finally, a comprehensive summary and review of the CVM were conducted by Egolfopoulos et al. [34].

Despite the breadth of work on the CVM, limited work has been done to understand the accuracy of the data reduction of CVM results for refrigerant-air flames, with their significantly reduced burning velocities. Hence, the present work aims to explore the effects of flame stretch, radiation, and extrapolation, as well as alternative data reduction approaches on the inferred burning velocity for these slow, more highly-radiating flames. The refrigerant adopted for the present work is R32 (CH_2F_2), a widely used refrigerant with an intermediate GWP of 677 and a reported peak laminar burning velocity in air of around 6 cm/s to 7 cm/s (at 298 K and 1 bar), an intermediate value as compared to other HFC refrigerants.

The approach in the present work is to generate pressure-time data using a 1-D numerical spherical flame simulation employing detailed kinetics and a radiation model, and then apply the data reduction approaches to the simulation data. In this way, the salient features of the flame are known, and their effects on the burning velocity inferred by means of different post-processing techniques can be explored. It is worth noting that the effects of buoyancy, ignition disturbances, instabilities, and wall effects are not the focus of this work and, hence, neglected in the simulations.

Although the burning velocity in the CVM arrangement can be extracted either using the time–pressure history $p(t)$ or the pressure $p(t)$ together with the measured flame radius history $R_f(t)$, only the former is considered in the present work. Data reduction for the numerical pressure-time data is accomplished using the recently developed, open-source software package CVDART (Constant Volume Data Reduction Tool) [35], which can use two-zone or multi-zone formulations via several approaches. Prior to discussing data generation and its analysis, a short description of the data reduction approaches is presented below.

2. Data Reduction

Through a thermodynamic analysis Fiock and Marvin [20] derived the following fundamental relation between S_u , $p(t)$ and $R_f(t)$

$$S_u(p, T_u) = \frac{dR_f}{dt} - \frac{R_v^3 - R_f^3}{3 p \gamma_u R_f^2} \frac{dp}{dt} \quad (1)$$

in which R_f is the flame radius, R_v the vessel diameter, and γ_u the ratio of the specific heats of the unburned gas, p the vessel pressure, T_u the unburned gas temperature and S_u the flame velocity with respect to the unburned gas. The following assumptions were made in the derivation of Eq. (1):

- (1) Ideal gas behavior,
- (2) Infinitely thin flame front,
- (3) Spherical flame front without instabilities,
- (4) Unburned gas (reactants) compressed at constant entropy (isentropic compression),
- (5) Unburned mixture is inert (no chemical reactions).

From Eq. (1) it is obvious that if the pressure and flame radius history are measured the burning velocity can be calculated directly. Alternatively, when only pressure is measured it is convenient to replace the flame radius in Eq. (1) by the burned gas mass fraction x_b which is defined as

$$x_b = \frac{m_b}{m_b + m_u} \quad (2)$$

where m_b and m_u are the mass of burned and the unburned gas in the vessel. The total mass, $m_b + m_u$, is a conserved quantity in the CVM. Using Eq. (2) and applying the isentropic relation $\rho_0/\rho_u = (p_0/p)^{1/\gamma_u}$ for the compression of the unburned gas leads to

$$S_u = \frac{R_v}{3} \left(1 - (1 - x_b) \left(\frac{p_0}{p} \right)^{1/\gamma_u} \right)^{-2/3} \left(\frac{p_0}{p} \right)^{1/\gamma_u} \frac{dx_b}{dt} \quad (3)$$

in which the subscripts b and u denote the burned and unburned gases, respectively, and 0 indicates an initial value. The ratio of the specific heat capacities of the unburned mixture γ_u can be deduced by knowing the reactant composition and using assumptions (4) and (5) (isentropic compression and inert unburned gas). Hence, the only unknown quantity in Eq. (3) is the mass fraction of the unburned gas.

As mentioned above, the relation between the burned gas mass fraction and pressure (or similarly time) must be derived in a data processing step and this is commonly done with a correlation as in refs. [32, 36] or with a simplified thermodynamic simulation, which is the approach adopted here. The post-processing or data reduction approaches are simplified simulations, in which only thermodynamic mixture properties are required and no detailed chemical kinetic model is needed. The post-processing approaches can be divided into two basic categories, the two-zone and multi-zone models. In the former, the gas in the vessel is divided into an unburned and a burned gas zone and both zones have uniform properties; in the multi-zone model the burned gas is subdivided into several zones or shells and each shell can have different mixture and thermodynamic properties. In both approaches, the mass and energy conservation equations are solved simultaneously. These equations are written as:

$$e = \int_0^{x_b} e_b dx + \int_{x_b}^1 e_u dx \quad (4)$$

$$v = \int_0^{x_b} v_b dx + \int_{x_b}^1 v_u dx \quad (5)$$

in which v and e are the total specific volume and specific internal energy in the vessel. The burned gas properties v_b and e_b are functions of the unknown burned gas temperature and composition, which are typically approximated by the equilibrium state (calculated at constant pressure and enthalpy) of the mixture. Equations (4) and (5) are solved iteratively for the burned gas temperature and the burned gas mass fraction. In the two-zone model approach, the conservation equations are solved for the entire burned gas zone, whereas in the multi-zone approach the equations are solved for the burning shells individually.

The two-zone model is limited since the burned gas is assumed to have uniform properties and its condition is determined by the solution of Eq. (4) and Eq. (5). Hence, anything that would change the burned gas thermodynamic properties, such as radiation or heat loss or gain, is neglected.

In the multi-zone model, however, modeling can be done in shells that are fully burned. For example, each shell experiences radiation heat loss which leads to a temperature gradient in the burned gas since the inner shells radiate for a longer time or the gas in the inner shells is compressed at different times, changing equilibrium in the burned shells as their temperature changes can also be included. Typically, energy fluxes (e.g., radiation) between shells are neglected because they are small, considering radiative heat transfer versus heat release rates. Different approaches for multi-zone models have been developed and are discussed here since they are employed in the analyses below to obtain flame velocities. The first, based on Elia et al. [25], is denoted in the present work as MECT (Mass and Energy Conserving Thermo) and the second, developed by Xiouris et al. [33], is the HTDR (Hybrid ThermoDynamic-Radiation). The main difference between the two approaches is that in HTDR no conservation equations are solved. Instead, an entire shell is burned at each pressure step. The burned gas state of the burning shell is estimated similarly as in the MECT model by the equilibrium state of the reactants. The burned gas occupies a larger volume after combustion which is compensated by compressing all the

previous burned shells and the unburned gas isentropically. This is done in an iterative way so that all shell volumes together add up to the vessel volume at the end. Hence, in the HTDR model, the shell volumes change continuously whereas in the MECT model they remain constant. After compression, the new value for burned gas mass fraction and flame radius can be calculated.

In HTDR, the pressure increase at each step is defined by the shell size whereas, in MECT, a pressure increment has to be defined. In MECT, during each pressure step, first, all shells are compressed isentropically, leading to updated shell temperatures. The actual burning shell is divided into a burned and an unburned part. The latter is similarly treated as the unburned gas outside of the burning shell and then the conservation equations are solved with the burning shell as the control volume. As explained above, the burned gas composition is estimated as that of thermodynamic equilibrium and the solution of these equations provides the burned gas temperature and burned gas mass fraction in the burning shell. With that, the overall burned gas mass fraction and the flame radius can be determined. Finally, the flame velocity can be calculated using either Eq. (1) or (3).

Note that the assumption of isentropic compression used in the data reduction models was tested by comparison of the results of the numerical simulations. The agreement between the predicted pressure and temperature from the equations for isentropic compression agreed very well with those extracted from the numerical results.

In the CVM, the expanding flame isentropically compresses the unburned gas so that analysis of the pressure rise data provides the experimental burning velocity as a function of the pressure and temperature in the chamber. While this is useful for providing data for applications such as piston engines and gas turbines, data at ambient conditions is typically required for refrigerant fire safety. Although the experiment is usually initiated under ambient conditions, the data at early times are not usable due to ignition disturbances, and large stretch effects due to small flame radii. Hence, data cropping and extrapolation to ambient conditions are necessary. In the literature, two functional forms for the extrapolation are suggested. The first is a power-law fit in pressure and temperature [24],

$$S_u = S_{u,0} \left(\frac{T_u}{T_{u,0}} \right)^\alpha \left(\frac{p}{p_0} \right)^\beta \quad (6)$$

$$S_u = U \left(\frac{T_{u,0}}{T_0} \right) \left(\frac{p}{p_0} \right)^\beta e^{-E_A/2\mathcal{R}_{fuel}T_{a,0}} \quad (7)$$

in which the subscript 0 denotes values at initial conditions. This equation is fitted to the experimentally measured or calculated flame velocity $S_u(p, T_u)$ with $S_{u,0}$, α , and β as fitting parameters. Another approach is to use an Arrhenius-like correlation as suggested by Lavoie [23]

In this case, the fitting parameters are U , β , and E_A . In thermal theory U and E_A correspond to pre-exponential factor and activation energy, respectively. Further inputs are the gas constant of the fuel \mathcal{R}_{fuel} and the adiabatic flame temperature $T_{a,0}$. As Metghalchi et al. [22, 24] described, this formulation might appear to be better from a fundamental perspective, but it has drawbacks. The correlation is very sensitive to the adiabatic flame temperature and hence to the thermodynamic data. The best fit fitting parameters often vary strongly and arbitrarily for similar data and are far from physically meaningful values. While there is no clear evidence in the literature on which correlation is

preferable, the power-law fit Eq. (6) tends to be used more often, perhaps because it is more straightforward to apply and is more robust. In the present work, however, both methods are used and compared since such comparisons have not been reported for refrigerant-air flames.

For the data reduction, the tool, CVDART developed at NIST [35], is employed. Three different models are implemented: a two-zone and two multi-zone models. The $S_u(p, T_u)$ data are fit with either the power-law or Arrhenius-type formulations, and the cropping limits of the initial and final data are varied to explore the influence on the extrapolation to ambient conditions. Finally, radiation heat losses are either included or neglected in the data reduction.

The influence of flame stretch is investigated by considering simulated flames for constant pressure conditions (at the p , T_u , and R_f condition of interest in the CVM experiment), for which both stretched and unstretched burning velocities can be obtained, as outlined below.

3. Simulation Framework

3.1 Code Description and Parameters

Simulations were carried out with the open-source code FlameMaster [37]. For the 1-D spherical flame formulation, the mass-, momentum-, energy-, and species-conservation equations are solved in a spherical coordinate system assuming ideal-gas behavior. First-order upwind and central differencing spatial schemes are employed with high-order implicit advancement in time. The species diffusion coefficients are determined by the Curtiss-Hirschfelder approximation and a mass correction is applied to the species diffusion velocities. The Soret effect was neglected. The reduced reaction mechanism of Burgess et al. [38, 39] for R32 (28 species and 90 reactions) was used; it gave equivalent results to those of the full mechanism for a number of test cases. The mechanism has been validated in the work of Burgess et al. [38, 39], and Hegetschweiler et al. [13, 15]. Further details on the verification of the FlameMaster code are provided in Ref. [40, 41].

The physical arrangement follows a CVM experiment at NIST [42]. The computational domain has an outer radius of 7.62 cm, at which wall boundary conditions are applied. To mimic the spark ignition in the experiment, the flame is initiated with a time-limited energy source term applied in a sphere with a radius of 3 mm. The time and absolute energy value of the spark were adjusted, depending on the reactant composition, initial pressure, and initial temperature, to provide flame propagation at near minimum ignition energy. The grid resolution required special consideration: in the constant volume setup, the pressure increases as the flame progresses, so that the flame thickness decreases (approximately linearly with the pressure increase). Grid convergence studies were conducted for the R32-Air flames which showed that 4000 to 5000 points are needed to properly resolve the flame front up to the highest occurring pressures. In this case there are always at least 30 points within the main reaction zone.

4. Results

The first part of the process in the current work is the generation of the numerical data (i.e., $p(t)$ data). Hence, FlameMaster simulations for the CVM configuration are conducted for CF₂H₂-air flames over a range of fuel-air equivalence ratio $0.9 \leq \phi \leq 1.4$, 298 K and 1 bar, and post-processed to obtain $p(t)$. Nonetheless, most of the discussion below focuses on results of a single equivalence ratio ($\phi=1.1$) since this is the equivalence ratio near the peak burning velocity [6, 12] and hence is the condition of most interest to the refrigerant safety community. Thus, unless otherwise noted, the results discussed below refer to $\phi=1.1$; results for the other ϕ are discussed at the end in the context of the inferred Markstein lengths and the extrapolated values of S_u . Simulations are conducted for both adiabatic (ADI) flames (no radiation) and for flames computed with an Optically Thin Model (OTM) for radiation. The

adiabatic simulations are discussed in detail below. The OTM results resulted in very similar conclusions; they are summarized after the adiabatic results and discussed in detail in the Supplementary Materials.

4.1 Adiabatic Simulation

For a given value of ϕ , an adiabatic numerical simulation was performed and $p(t)$ is obtained. To calculate $S_u(p, T_u)$, the Fiock-Marvin formulation Eq. (1) is used together with the relevant parameters in Eq. (1). This result is referred to in the present paper as the Fiock-Marvin result or the so-called “exact” solution. Note that this method is similar to an experiment in which both pressure and flame radius history (via an optical system) are measured. Figure 1 shows $S_u(p, T_u)$ from this exact solution as the solid red line. For comparison, also shown are the results of laminar unstretched 1-D planar simulation at the different values of p and T_u . As the figure shows, for pressures greater than $2p_0$, the two flame velocity curves have a similar variation with p ; however, values from the spherical simulation are about 2 % to 3% shifted upwards as compared to the planar calculations. As described below, for the larger pressure and radii flames the stretch effect is small, so the difference between the planar and spherical results, although small, is unexpected. This difference is not likely from ignition disturbances since, at early times in the CVM, there is a significant time for flame growth and dissipation of the ignition effects before an appreciable increase in pressure occurs. For example, at a pressure of $2p_0$, R_f has already reached approximately 5.9 cm as compared to the simulated ignition kernel of 0.3 cm. Also, numerical experiments were performed in which the ignition energy was varied by several orders of magnitude to ensure that the values used had no effect on the subsequent flame propagation. As further investigation, a variety of isotherms were used for tracking the flame location history, and while they did have a minor effect, it was not large enough to account for the 2 % to 3 % difference. Nevertheless, for lower pressures, the planar and spherical burning velocities clearly diverge, and this deviation may have an effect on the extrapolation of S_u to initial conditions. Hence, the two cases: non-extrapolated data at higher values of p and T , and the extrapolation to initial conditions are discussed separately.

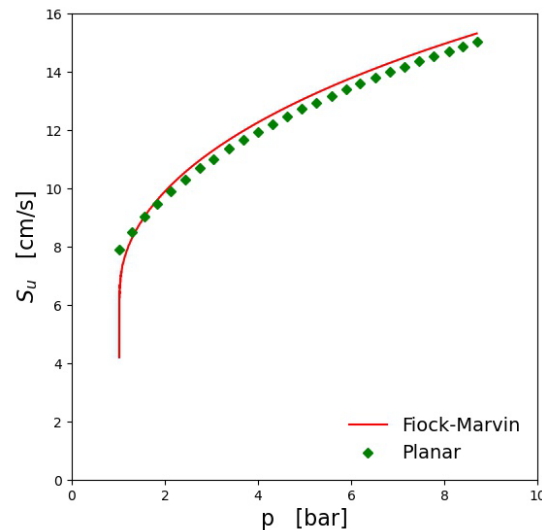


Figure 1: Comparison of planar and spherical constant volume simulations under adiabatic conditions $p_0 = 101325$ Pa, $T_0 = 298.15$ K, and $\phi = 1.1$.

4.2 Non-Extrapolated Results ($P/T > p_0/T_0$)

The performance of different data reduction models for reproducing the exact solution is shown in Figure 2. As discussed above, three different models are applied: A two-zone and two multi-zone models (MECT and HTDR). Figure 2 depicts these results together with the “exact” Fiock-Marvin and the planar values as in Figure 1. Only the curve from one multi-zone model (MECT) is shown here because the two multi-zone models give indistinguishable results. Radiation was not considered in the data reduction models since the simulations were performed at adiabatic conditions. The multi-zone models reproduce the Fiock-Marvin solution accurately, validating the data reduction approaches. There is a slight error at p close to p_0 (around 2.5%) which drops below 1% at about $1.35 p_0$ and then levels off at about 0.1%. The larger error at p near p_0 is most likely due to the assumption of an infinitely thin flame in the data reduction model; this assumption is good for larger flames (and higher pressure) since the flame thickness decreases with increasing pressure, but is less good for the small, near ambient pressure flames. Also, the data reduction model does not capture the effects of the ignition process that initiates the flame in the simulation and these are more important for smaller flames.

The data reduction using a two-zone model, even for this adiabatic condition, shows some deviation from the exact Fiock-Marvin solution obtained from the simulation. At p near p_0 , the two-zone data reduction model closely follows the multi-zone models but starts to deviate with increasing pressure, reaching a value that is 3.5 % lower than the exact solution at $p = 8p_0$ (note that this pressure is not relevant to experiments since wall effects occur at a smaller pressure rise). That is the consequence of the models’ different treatment of the burned gas region. In the multi-zone approach, the non-uniform burned gas properties are approximately resolved, whereas in the two-zone model, constant values are assumed. The greatest influence on the prediction of burning velocity comes from the burned gas temperature since it largely (besides the mixture composition) determines the fluid density which in turn determines the flame radius evolution with increasing pressure. Examination of the numerical results indicates that there is a gradient of temperature in the burned gas region (even for the ADI case), and hence the multi-zone data reduction scheme is more accurate. Heat conduction in the burned gases is too slow to equalize the temperature gradient. Thus, a first observation is that for such slow-burning flames, even with no radiation, the two-zone model, unlike the multi-zone models, applied to pressure-rise data does not reproduce $S_u(p, T_u)$ as obtained in the numerical simulations. While this error in the two-zone model is not overwhelmingly large, it is important to keep it in mind for kinetic model development since most of the data in the literature for refrigerant-air burning velocities has been obtained with the CVM method using a two-zone model for data reduction, and it has been suggested to use higher p/T_u data [12] for model validation since then an extrapolation is not required.

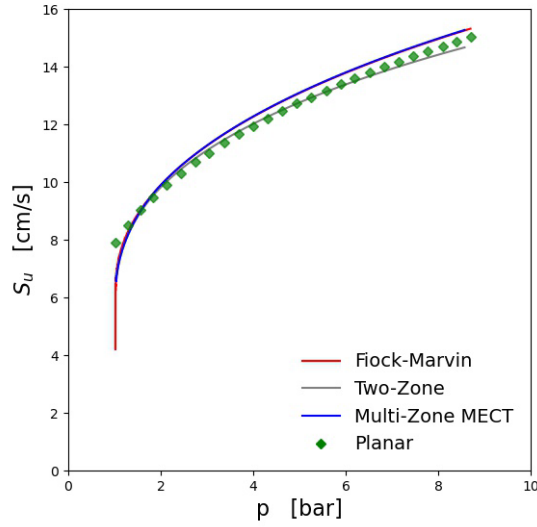


Figure 2: Comparison of planar and spherical constant volume simulation with extracted S_u from two-zone and multi-zone (MECT) data reduction models.

The influence of flame stretch is investigated by considering simulated spherical constant pressure flames for conditions of p and T_u along the $p(t)$ curve. Starting at the initial condition (here standard conditions of 1 bar and 298.15 K), for each p and T_u condition (which corresponds to a particular flame radius in the CVM) we perform a separate CPM simulation for a spherically-expanding flame and compare the stretch-affected burning velocity to the corresponding CVM result at the same p , T_u , and flame radius. This process is then repeated for successively larger flame radii, i.e., p/T_u , along the isentrope of the CVM simulation. Thus, from each CPM simulation, we obtain an estimate of S_u for both the stretched and unstretched (via extrapolation back to zero stretch) condition; i.e., each CPM simulation approximates S_u at the instantaneous p , T_u , and R_f for each point selected from the CVM run.

The procedure is outlined with the help of the two plots in Figure 3. The left frame of Figure 3 shows R_f as a function of p along the isentrope of a CVM simulation, and from it a particular p/T_u condition (for example, each of the colored points) is selected, starting at p_0/T_0 , and the corresponding flame radius of a CVM flame is determined. For each p/T_u condition, a CPM calculation is performed, providing curves of S_b versus stretch rate κ as shown in the right frame of Figure 3, where S_b and κ denote burning velocity with respect to the burned mixture and the stretch rate. For each p/T_u condition, the stretch rate of the CVM simulated flame is calculated via [43]:

$$\kappa = \frac{2}{R_f(t)} \left(\frac{dR_f(t)}{dt} \right) \quad (8)$$

Finally, the stretch-affected burning velocity at this value of R_f (or κ) is extracted using the $S_b(\kappa)$ curves in the right plot of Figure 3; i.e., at each of the closed symbol locations in the figure. Note that this approach leads to slightly different stretch rates in the CVM and CPM flames because the dR_f/dt values at the respective flame radius are not exactly the same (due to compression-induced fluid motion in the CVM) and this affects the stretch rate as given in Eq. (8); however, this is a good approximation for the present purpose as the difference is expected to be minor. Furthermore, using the non-linear correlation [44] indicated by the dashed lines in the right plot of Figure 3, the values of the zero stretch flame velocities (indicated by the open symbols) are obtained by extrapolation.

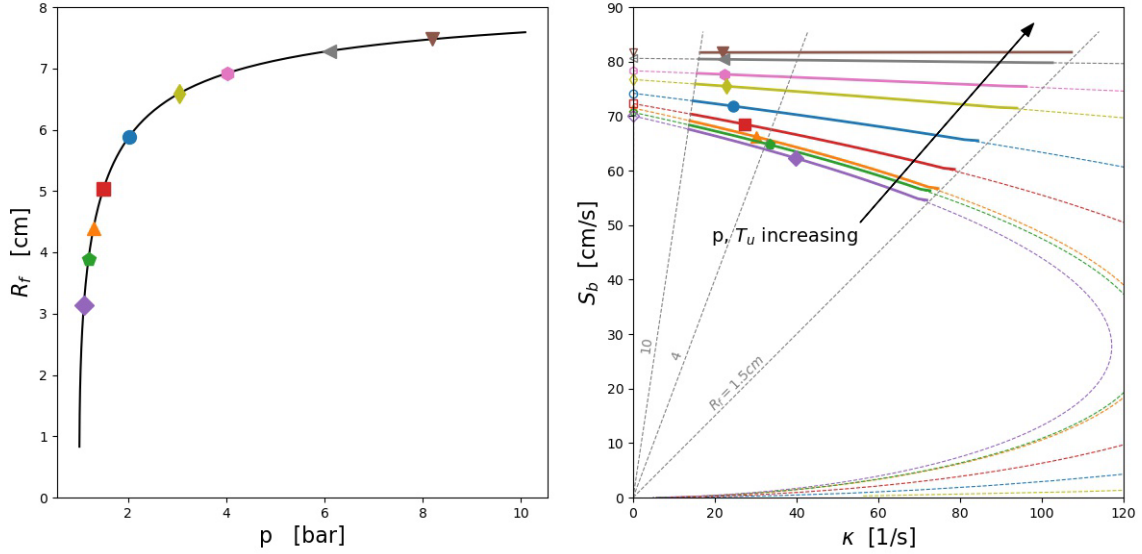


Figure 3: Left frame: Flame radius $R_f(p)$ vs. pressure along an isentrope from the CVM simulation. Right Frame: curves of the burned gas burning velocity S_b vs. stretch rate κ from a CPM simulation for each p/T_u condition as indicated by the solid points in the left frame. The location of the solid symbol on each curve in the right frame indicates the appropriate value of κ (i.e. R_f) for S_b determination at the stretched condition; the open symbols denote the burning velocity at the unstretched ($\kappa = 0$) condition for that value of p/T_u . (R32/air flame at $\phi=1.1$)

For each p/T_u pair in Figure 3, Figure 4 shows the resulting stretched (circular symbols) and unstretched (square symbols) CPM calculated burning velocities. Also shown is the exact Fiock-Marvin (solid line) burning velocity extracted directly from the CVM simulation. Comparing the stretched and unstretched CPM results, it is obvious that near the initial conditions, the stretch influence is quite large and decays as the flame grows and pressure increases (i.e., the stretch rate decreases). Note that this result is expected since in Figure 3 (right frame), the $S_b(\kappa)$ curves for lower pressures (smaller R_f) are much steeper (larger Markstein length) and therefore the difference between stretch affected and zero stretch values is larger. Thus, the difference between the two sets of points in Figure 4 provides insight into the effects of stretch in this configuration and becomes an issue in the selection of the data range used in the curve fits for the extrapolation, as described below.

At $p=1$ bar, the stretched value of S_b is about 45 % lower than the unstretched value, while above 2 bar the relative error is below 3 % and then decays to zero at ≈ 6 bar. Thus, comparing these stretched and unstretched CPM results to the Fiock-Marvin results (solid red line) for the CVM simulation it seems likely that the steep drop in the curve towards low pressure is due to stretch effects. As mentioned above in the discussion of Figure 1, the CVM simulated burning velocities, i.e., the $S_u(p, T_u)$ curve, is slightly larger than the burning velocities of the planar flames at $p > 2p_0$. This is also the case here in Figure 4: the Fiock-Marvin results for the CVM (solid red line) are slightly shifted upward relative to CPM simulated stretched values (to which they should be compared). This seems to be a systematic error of the simulation and the reason is unknown, as discussed above. However, if the Fiock-Marvin curve from the CVM simulations were to be shifted down by ≈ 3 % it would agree with the stretch-affected CPM simulated burning velocities very well, supporting the conclusion that the CVM results are stretch affected at $p < 2p_0$.

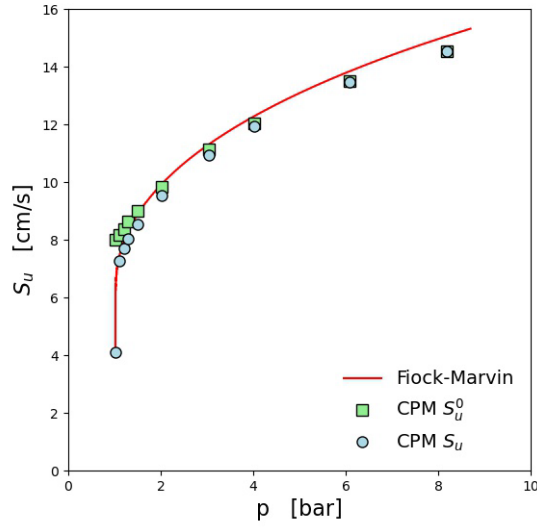


Figure 4: Comparison of Fiock-Marvin extracted flame velocity (red line) from the CVM and results from CPM simulations; square symbols: stretch extrapolated (zero stretch) values, circular symbols: stretch affected values, all along an isentrope starting at p_0/T_0 .

4.3 Extrapolated values

As mentioned previously, ambient conditions are of most relevance to the refrigerant safety community. Hence, an extrapolation of the CVM $S_u(p, T_u)$ results back to the initial test conditions, which are usually near ambient, is required. Given the ignition disturbances in the experiments [12, 45], and the stretch effects at early times noted above, cropping of the initial phase of the pressure trace is typically required. The use of numerically generated pressure-rise data in the present work allows one to isolate just the effects of stretch on the extrapolation accuracy using the variety of data reduction approaches outlined above. Figure 5 shows the error caused by the extrapolation of the extracted $S_u(p, T_u)$ data at higher p/T_u (i.e., data in Figure 2) back to p_0/T_0 , as a function of the lower limit for the data cropping. Results are shown for the various data reduction schemes (Fiock-Marvin, two-zone, and multi-zone MECT, adiabatic). The lower set of curves (solid lines) refer to a power-law fit to $S_u(p, T_u)$ and the upper set of curves (dashed lines), to an Arrhenius fit. Data are presented as the extrapolated burning velocity (to 298 K, 1 bar) normalized by the value for a planar flame at p_0/T_0 . Note that each point in the figure is an extrapolated value of S_u (then normalized) which is obtained from the curve fit over the data range defined by the indicated (x-axis) lower crop limit in the figure. The planar value is the most suitable normalization value since all others are affected by their curve fit. The dependent variable in the figures is the lower crop limit expressed as p/p_0 , i.e., data at p below p/p_0 are excluded. For the spherical data, the Arrhenius correlation leads to larger extrapolated values than the power-law, and the results of both are somewhat dependent upon the lower crop limit.

Also shown are the results of fitting a curve to the planar flame burning velocity data $S_u^0(p, T_u)$ along the isentrope. Both the power-law and the Arrhenius fits yield $S_u^0/S_{u,planar}^0=1.0$ at $p/p_0=1.0$, as expected. Qualitatively, these traces are different since all values are stretch-free.

To quantify the quality of the least square fits, the overall root mean square (RMS) errors are depicted in the right frame of Figure 5. The power law better approximates the data for all base traces and for all crop limits. The large RMS error when a lower cropping limit is used illustrates that both fits do not work well when the stretched data are included. Similarly, the very low RMS errors for the planar data illustrate that both fit types follow $S_u^0(p, T_u)$ very accurately for unstretched data over the T and p of

the simulations, justifying the use of the curve fits in the extrapolations. Moreover, the residuals of the fit to the MECT obtained data as a function of p are depicted in Figure 6, which shows that both the power-law and Arrhenius formulations fit the data less well at low pressure (i.e., small radii flames, which have higher stretch), and that the residuals are more uniformly distributed if the smaller radii data are eliminated (i.e., higher lower crop limit).

As noted above, there is a 2 % to 3 % positive offset in the spherical data for larger flames relative to the planar values, as can be seen in Figure 1 (considering only the power-law fit results). As p/p_0 decreases towards unity, the offset becomes about 4 %. Considering the disagreement between the two-zone and multi-zone results in Figure 2, it is a bit surprising that the two give basically the same extrapolated values. As seen in Figure 2, the two-zone and multi-zone traces significantly deviate only after $2p_0$, so the extrapolation towards lower pressure values is guided in a similar way for the two data reduction models.

The results with respect to the appropriate lower cropping limit for the present R32-air flames are in line with those of other researchers, who reported results for other fuels and burning velocity ranges; e.g. Xiouris et al. [2016] recommend to use $2.5p_0$ as cropping value, and Chen et al. [46] recommended $2p_0$. In the present work, cropping the $S_u^0(p, T_u)$ data at the approximately $1.75p_0$, the power law extrapolation leads to S_u values close to the 1-D planar result. Note that this value is slightly lower than the stretch analysis above suggests (around $2p_0$), and lower than Xiouris et al. [33] suggest; however, this is likely due to the overprediction of the constant volume flame velocity by 2 % to 3 % compared to the 1-D planar results (see Figure 1). If the cropping limit were as low as $1.25p_0$, a value near that used in some previous works [6, 12], the extrapolated burning velocity would be lowered by 5 % to 6 % as compared to the planar adiabatic value. While it seems clear that lower cropping limits at least above $2p_0$ seem appropriate, the present analyses were extended below this value since quite a bit of data in the literature has been reduced with lower crop limits, and it seemed useful to quantify the effect of those lower cropping limits.

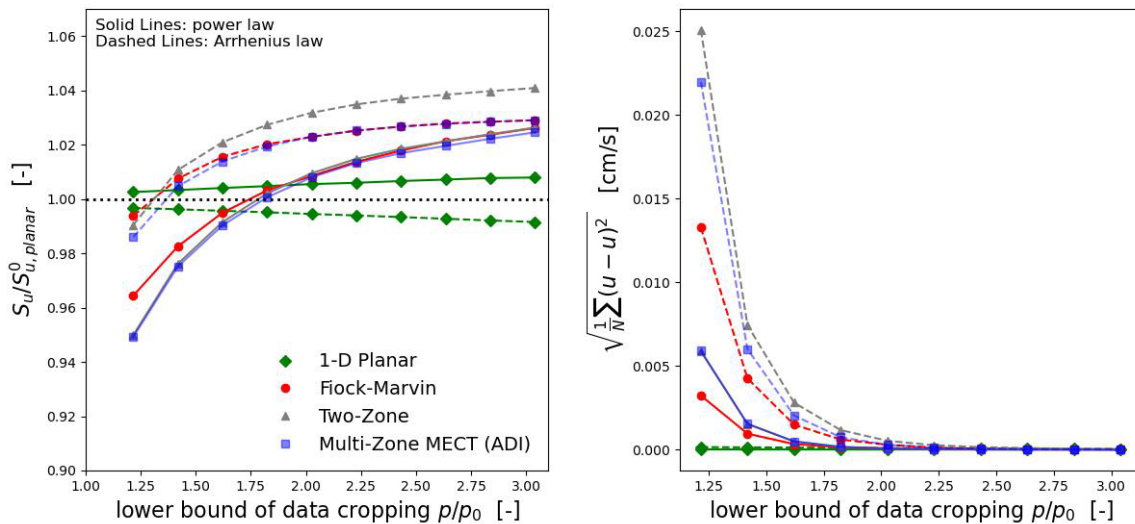


Figure 5: Relative error (left frame) of extrapolated flame velocities as a function of the lower pressure cropping limit of the data (p/p_0). Results shown for: Fiock-Marvin, two-zone, and MECT multi-zone data reduction; solid lines: power-law fit, dashed lines: Arrhenius fit. The reference value is that of a 1-D planar flame at standard condition. Right frame, standard error of fit. ($\phi=1.1$, $T_0=298$ K, $p_0=1$ bar).

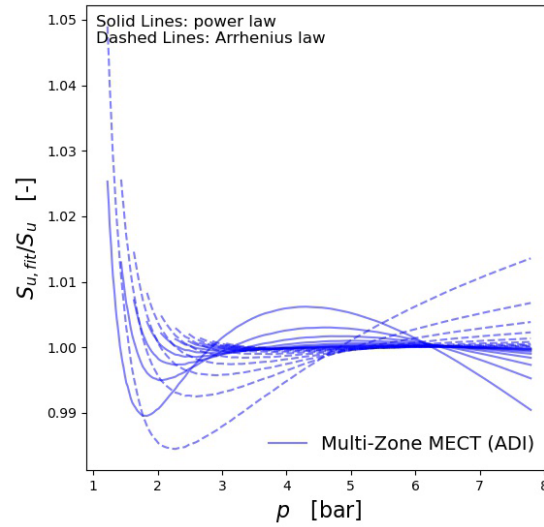


Figure 6. Residual of fit presented as $S_{u,fit}/S_u$ for $S_u(p, T_u)$ as a function of p for data reduced using the multi-zone MECT model with adiabatic conditions. Different curves show data for fits with lower cropping limits of the fit as indicated by the starting point of each curve.

An alternative way to avoid extrapolation to standard conditions is to start the simulation (or experiment) at lower pressure and temperature on the same isentrope as standard pressure and temperature. This approach has been described previously by Metghalchi and Keck [24]. Figure 7 shows a CVM simulation initiated at $p_0 = 0.69$ bar and $T_0 = 270$ K (dashed line) and the standard CVM simulation (solid line). Additionally, the 1-D planar value at standard condition is shown (diamond symbol). When the CVM flame starting at lower p/T arrives at the standard condition (1 bar, 298 K) ignition effects have nearly completely decayed and stretch effects are mostly gone since the flame radius is larger. From Figure 4, it can be estimated that the relative error due to stretch at 1 bar (which is equal to $1.4 * 0.69$ bar), is about the same as in Figure 7; i.e., the results in Figure 4 and Figure 7 are consistent. Nonetheless, in such experiments, ignition of the refrigerant-air mixtures may be more difficult at the lower pressure and temperature, and the higher required ignition energies could disrupt the initial flames more. In the numerical simulations, we verified that the ignition energies used did not affect the flame propagation (via tests with ignition energies varying by more than a factor of ten).

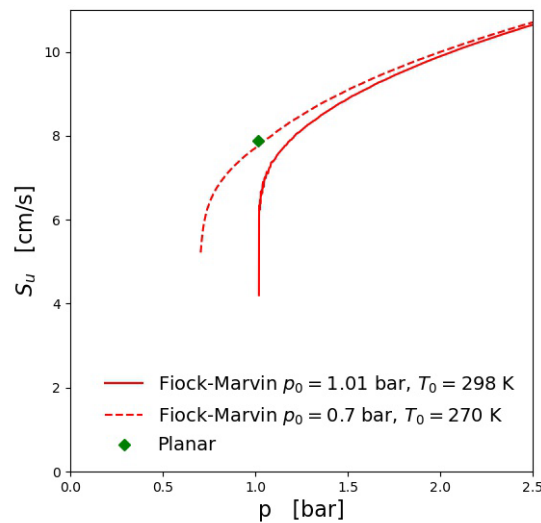


Figure 7: CVM simulations starting at standard condition (solid line) and lower pressure and temperature, i.e. 0.69 bar and 270 K (dashed line), and the 1-D planar burning velocity at standard

conditions. The $p(t)$ data from the CVM simulations were post-processed by applying the Fiock-Marvin formulation.

4.4 Results for a range of equivalence ratios

In the discussion above, for clarity, only the equivalence ratio, $\phi=1.1$, that represents the peak burning velocity for R32/air flames, was considered. Herein, the same data reduction process is applied to numerically generated synthetic data for R32/air mixtures with $0.9 \leq \phi \leq 1.4$. For extrapolation, the power-law and Arrhenius fits are applied and the lower crop limit is chosen as $2p_0$, since this value is suggested (for $\phi=1.1$) by the CPM stretch analysis described above. Figure 8 shows, for a range of equivalence ratio, the results from the extrapolations of the $S_u(p, T_u)$ data extracted from the pressure rise data from the CVM simulations using the Fiock-Marvin, the two-zone, and the multi-zone MECT approaches. Also shown are the steady 1-D planar results and for comparison the results of a CPM simulation (at 298 K, 1 bar initial conditions) extrapolated to zero stretch. In Figure 8, a lower cropping limit of $2p_0$ was used for the $p(t)$ data; using $2.5p_0$ gave very similar curves, as did using $1.2p_0$, although for the latter, the spread in curves for the $\phi=0.9$ mixtures was about twice as large and that for the $\phi=1.4$, about half as large, as for the $2p_0$ case. Note that the scale in Figure 8 is expanded to show the differences between the curves; the differences, however, are small relative to the magnitude of S_u .

For the entire range of ϕ , the planar and CPM (unstretched) results are very similar with a slight deviation at higher equivalence ratios. As expected, the CVM Fiock-Marvin and multi-zone burning velocities are also very close to each other. Nonetheless, the curves for the CVM results (MECT and Fiock-Marvin) in Figure 8 are somewhat tilted relative to the stretch-free results (the 1-D planar and CPM), the former being slightly lower on the lean side and slightly higher in the rich side. This can be explained by considering that as discussed previously for CPM results [15], the Markstein numbers of the lean flames are much higher; i.e., the stretch effect becomes larger for leaner flames.

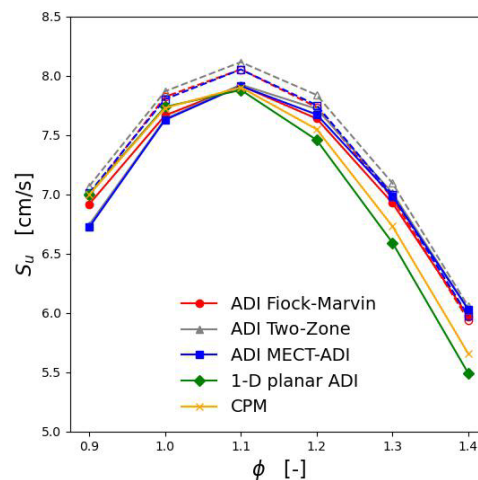


Figure 8: Simulated flame velocities at standard conditions for a range of equivalence ratios. The CPM results are stretch corrected (extrapolated to zero stretch) and the CVM values (Fiock-Marvin and multi-zone MECT, and two-zone) are obtained by the power-law extrapolation (to 298 K, 1 bar) and using a lower crop limit of $2p_0$ for all equivalence ratios. Dashed lines: Arrhenius fit; solid: power-law fit.

Because the effects of stretch on S_u varies with equivalence ratio, the lower crop limit of the $p(t)$ data that gives agreement of the extrapolated S_u with the planar value depends upon ϕ . Following the presentation as in Figure 5 for $\phi=1.1$ (left frame), Figure 9 presents for a range of ϕ , the error in the extrapolated S_u as a function of the lower crop limit, although in Figure 9, the data are reduced only using the Fiock-Marvin formulation. As in Figure 5, data are extrapolated using both the power-law and Arrhenius fits; only the former are discussed here since they better fit the $S_u(p, T_u)$ data. As indicated, for $\phi=1.1$, the lower crop limit of $2p_0$ provides good agreement with the planar S_u ; however, using this value for $p(t)$ data for other ϕ leads to errors of about -3 % to +8 %, for ϕ from 0.9 to 1.4, respectively. This analysis indicates that ideally, the lower crop limit could be made dependent on the strength of the influence of stretch (basically Markstein length). For example, for $\phi=0.9$, a lower crop limit of $3p_0$ gives no error, while for $\phi=1.4$, a value of $1.25p_0$ gives an error (the minimum error) of +4 % but an error of about +10 % (the maximum error) at a lower crop limit of $3p_0$. Thus, even for analysis of $p(t)$ data synthetically generated (i.e., clean, no buoyancy, no radiation, little ignition effects, spherical, etc.), there is a tradeoff in selection of the lower cropping limit, and for this case, choosing $2p_0$ seems reasonable since it gives the correct value for the peak S_u , and tolerable errors for the other ϕ . The need for differing lower crop limits for different values of ϕ results from the relatively high sensitivity to stretch (Markstein length) for the lean flames of R32 with air, as has been discussed previously [15]. The lean flames are too stretch affected at small times (small radii) in the present flames for the data at short times to be included in the data used for the extrapolation curve-fitting. The richer flames are not strongly affected by stretch, so the most accurate data for extrapolation includes the small radii data, which are closer to ambient conditions to which the extrapolations from the curve fit are directed. For some flames (although not R32-air flames), transition to cellular flames can occur for rich conditions, so much of the higher-pressure data would be cropped out and hence using more of the low-pressure data can be important for providing enough data for a good curve fit.

Such fits were suggested by Keck and others and fairly widely adopted, mostly for convenience. It is fortuitous that these fits can be used to extrapolate to ambient conditions, and the goal in the present work was to assess their accuracy in the present refrigerant-air flames. While it would be interesting, from a fundamental perspective, to understand why the power-law or Arrhenius fits to the $S_u(p, T_u)$ work or do not work, that is beyond the scope of the present paper.

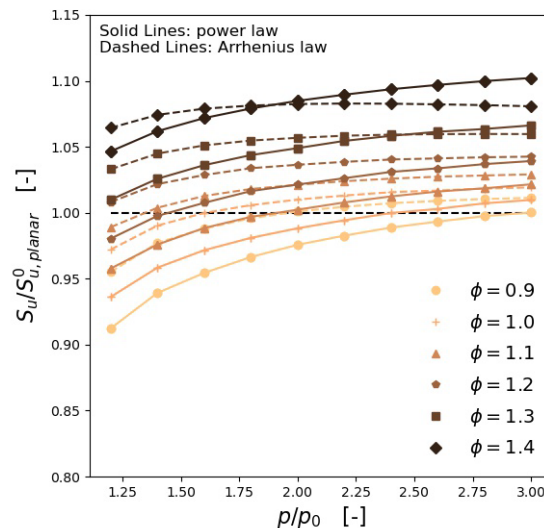


Figure 9: Relative error of extrapolated flame velocities as a function of the lower pressure cropping limit of the data (p/p_0), for a range of ϕ . Results shown for Fiock-Marvin data reduction of ADI generated $p(t)$ data; solid lines: power-law fit, dashed lines: Arrhenius fit. The reference value is that of a 1-D planar flame at standard condition. ($\phi=1.1$, $T_0=298$ K, $p_0=1$ bar).

5. OTM Simulation

The analyses performed above for adiabatic conditions (ADI) were repeated but including radiative heat losses from the hot, burned gases. The numerical simulations employed to generate the $p(t)$ profiles thus include an Optically Thin Model (OTM) for radiation that accounts for emission from the major radiating species (CO_2 , CO , HF , H_2O , and COF_2), but neglects radiation re-absorption by the burned or unburned gases. The detailed results are presented in the Supplementary Materials. While the exact numbers for the results are slightly different, all of the conclusions from the adiabatic results are qualitatively the same for the results including OTM radiation. For the extrapolated results, Figure 10 below for the OTM results shows the equivalent results as in Figure 8 for the ADI conditions.

The Fiock-Marvin and MECT curves show the same behavior as seen in the adiabatic case, although the curves are shifted to slightly higher values relative to the planar case since the selected lower crop limit generally leads to burning velocities that are too high (and the effect is stronger for richer flames, as described in the Supplementary Materials section below). For $\phi=0.9$, the spherical results are closer to the planar values (<1 % difference) and for $\phi=1.4$, about 16 % higher. The reason is the same as for the adiabatic flames: the lean flames are more affected by stretch and need a higher crop limit than the rich flames. Nonetheless, all post-processing techniques yield similar results unless using the two-zone model as it cannot account for radiation. The extrapolated results from the two-zone model for richer mixtures are not as far from those of the other formulations as they are for leaner conditions. This is coincidental and has to do with the nature of the power law fit and the detailed shape of the velocity trace. Generally, in terms of reducing $p(t)$ data to obtain $S_u(p, T_u)$, it is clear that the multi-zone MECT (or HTDR) model leads to the most accurate results, which are very close to those of the exact (Fiock-Marvin) results from the simulation.

The agreement between the CPM and 1-D planar-derived results is not as good as in the adiabatic case. Here the CPM values are shifted upwards by 4% over the whole range as compared to the planar ones. The reason is most likely because the estimation of the burned gas density for the conversion of S_b to S_u is not exact. This issue is described in more detail in the description of Figure 15 in the Supplementary Materials. There, it is found that the values of S_u under OTM conditions are 0.94, 0.96, and 0.88 those for adiabatic conditions for $\phi=0.90$, 1.1, and 1.4.

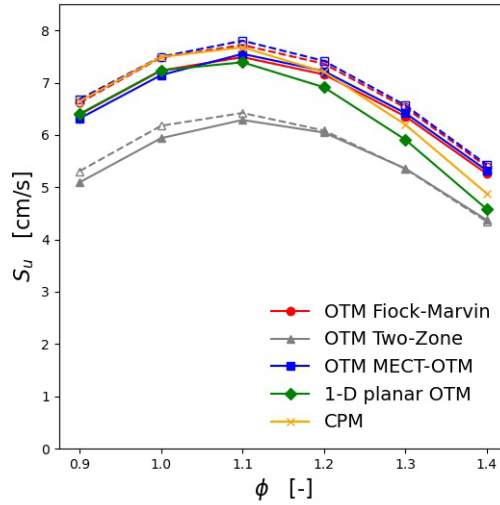


Figure 10: Simulated flame velocities at standard conditions for a range of equivalence ratios. The CPM results are stretch corrected (extrapolated to zero stretch) and the CVM values (Fiock-Marvin, multi-zone MECT, and two-zone) as well as the 1-D planar simulations are obtained by the power-law extrapolation (to 298 K, 1 bar) and using a lower crop limit of $2p_0$ for all equivalence ratios. Dashed lines: Arrhenius fit; solid: power-law fit.

6. Ramifications for Experimental Data Reduction

While the above discussions quantified the errors from stretch, radiation, and extrapolation for synthetic $p(t)$ data, it is useful to explore the implications for application of the techniques to experimental data. These effects will be present in both numerical and experimental results, and it seems useful to first examine them in simulated data since experimental data will have the additional complications related to ignition disturbances, non-symmetrical ignition, igniter heat losses, buoyancy, confinement effects, unknown wall reflectivity, and wall heat losses for large flames.

The most important uncertainty described in the present work is related to radiation heat losses. This is summarized in Figure 11, which shows S_u as a function of pressure for a simulated R32/air CVM flame. The solid lines represent simulations with (OTM) or without (ADI) radiation is used to generate the $p(t)$ data, which are then analyzed with the MECT data reduction scheme, in each case using the proper radiation model that was used to generate the $p(t)$ data. As described above, these results are coincident with the results of a Fiock-Marvin (exact) analysis of the output of the simulation (which for clarity are not shown in Figure 11). As shown in the figure, the effect of radiation on the S_u is minor. Nonetheless, if the incorrect radiation model is used to analyze the $p(t)$ data, the results are as shown by the dashed lines. Hence, very large errors can occur if the wrong radiation model is applied. While application of a numerical simulation employing a detailed radiation model [16, 47] is desirable, the narrow-line parameters for R32/air flames have not yet been generated. Since it is not known a priori which radiation treatment is closer to reality, it seems reasonable in reducing experimental $p(t)$ data to apply both the ADI and OTM formulations in the MECT data reduction scheme and then average the S_u obtained from the two. This would produce a maximum error of half the difference between the solid and dashed lines in Figure 11. This is particularly important if data at higher p/T are used for model validation, as has been suggested in previous work [12]. For example, as indicated in Figure 11, at $p=3$ bar, the error due to unknown radiation in the experiment can cause an uncertainty of about $\pm 21\%$ in S_u at $\phi=1.1$.

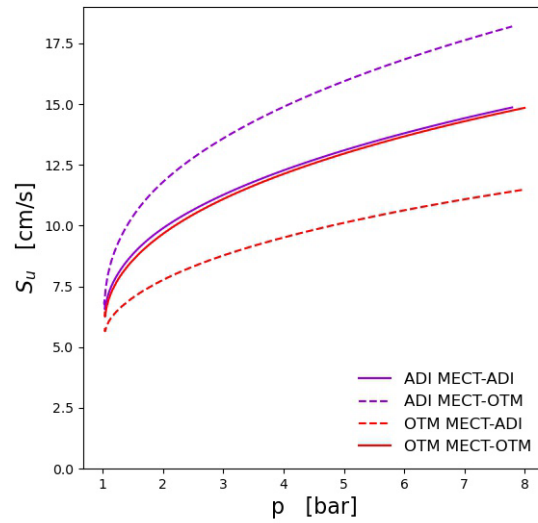


Figure 11: S_u as a function of pressure from analysis of the $p(t)$ data from a numerical simulation of an R32/air CVM flame, with (OTM) and without (ADI) radiation heat losses. Solid lines are for an MECT data reduction using the same radiation model as was used to generate the $p(t)$ data; dashed lines are the result when the incorrect radiation model is employed.

The two-zone data reduction models should not be used until the radiation occurring in the experiments is better understood. Two-zone models are inferior in all cases, can lead to large errors if OTM radiation is most applicable, and application of the multi-zone models is relatively straightforward [35].

Power-law curve fits are preferred over Arrhenius fits for R32/air flames in the CVM experiments since the former fit the data better and their extrapolation error is less sensitive to the lower cropping limit.

The next consideration addressed in the present work is the effect of the lower crop limit on the extrapolated S_u . While the experiments typically have noise associated with the ignition [12], the cropping required to eliminate the noise ($\approx 1.25p_0$) is typically less than that desired from a stretch consideration ($\approx 2p_0$). Nonetheless, a lower crop limit of $2p_0$, while apparently acceptable for $\phi=1.1$, causes errors in S_u for richer flames of up to 14 %. It is thus recommended that in reducing experimental data, the lower crop limit is adjusted to be higher for lean flames and lower for richer flames (for large molecular weight fuels. Results for CH_4 or NH_3 fuels would be the opposite). This can be accomplished by picking a lower crop limit and looking at the quality of the fit and adjusting the lower crop limit until the residuals are random. This is relatively straightforward using software now available [35]. This will be particularly important for experimental data since rich mixtures sometimes transition to cellular flames, and the required upper cropping limit can limit the available data for the curve fit.

The present results indicate that use of the extrapolated S_u is better for model validation since the errors from unknown radiation there are only about 6 %, 4 %, 12 % at $\phi=0.9$, 1.1, or 1.4 (OTM vs. ADI assumption in the data reduction) but can be up to about 45 % different at 3 bar.

7. Conclusions

The purpose of the present work was to quantify, for R32/air flames, the accuracy in obtaining the laminar unstretched burning velocity $S_u(p, T_u)$ data from pressure-time history data $p(t)$ in a Constant Volume Method CVM experiment. The errors examined in the present work included those caused by stretch, radiation, and extrapolation to the initial conditions of the mixture, as well as the accuracy of several data reduction approaches. To isolate these effects, the data reduction techniques were applied to idealized $p(t)$ data synthetically generated from a numerical simulation, which also allowed determination of the $S_u(p, T_u)$ for comparison with the inferred results. The major conclusions of the work are as follows.

1. Analysis of $p(t)$ data generated from a detailed numerical simulation of a CVM experiment for R32/air mixtures at 298 K and 1 bar using a multi-zone model (HTDR or MECT) can reproduce the $S_u(p, T_u)$ data obtained from the numerical output very accurately, generally within about 1 %, validating the technique as a method of flame speed determination for these mixtures.
2. Estimating the radiation heat losses in the experiment is very important in the data reduction. At higher T/p (3 bar to 5 bar), neglect of radiation can lead to errors of up to 45 % (OTM vs ADI assumption in data reduction, $\phi=1.1$, R32-air flames). Note that radiation effects will be more important for richer flames for which the concentration of radiating species in the products is higher and radiation heat losses are a higher fraction of the heat release rate (which scales with the burning velocity).
3. In lieu of knowing the proper radiation model to apply, it is recommended that both OTM and adiabatic formulations of the multi-zone data reduction model be applied and the results averaged. For $\phi=1.1$, this will give results that are at most ± 2 % in error for the extrapolated values of S_u and ± 22 % for higher T/p (3 bar to 5 bar). Hence, until radiation effects are better understood, extrapolated S_u to ambient conditions are better for model validation. Note that this is in contrast to the recommendation in [12].
4. For R32/air flames at $\phi=1.1$, stretch effects are important for small flames, yielding a relative error of about 21 % at $1.025p_0$ and 45 % at $p=p_0$.
5. For R32/air flames at $\phi=1.1$ flames, a lower crop limit of $2p_0$ is recommended to eliminate stretch effects on the extrapolated S_u values.
6. Extrapolation to obtain S_u at ambient initial conditions worked reasonably well, with errors of -4.5 % to +2.5 %, for low pressure crop limits of $1.25p_0$ and $3.0p_0$, respectively (for $\phi=1.1$ flames).
7. Use of a constant lower crop limit of about $2p_0$ is reasonable for near stoichiometric R32-air flames and leads to small errors, but for rich flames, can lead to errors of up to 14 %. For most accurate values of S_u for lean and rich flames, the lower crop limit should be adjusted manually. This is especially important for experimental data since wall effects or flame acceleration may require a relatively low upper crop limit. A constant lower limit for all values of ϕ , while desirable, can sometimes lead to a very small useable data range for rich flames, and manual selection of the crop limits can help preserve useful data. The optimum lower crop limit for other fuels is unknown.
8. For the extrapolation, a power-law curve fit to the $S_u(p, T_u)$ data is preferred over an Arrhenius fit since it follows the data more accurately.

Acknowledgements

The authors obtained financial support under contract DE-EE0007615 from the Office of Energy Efficiency and Renewable Energy, U.S. Department of Energy, Buildings Technologies Office (Project Manager Antonio Bouza), as well as from the U.S. Department of Defense, Strategic Environmental Research and Development Program (SERDP), project WP-2740, with Robin Nissan serving as Project

Manager. Helpful conversations with and exploratory simulations by Prof. Chen are gratefully acknowledged.

References

- [1] G. J. Velders, A. R. Ravishankara, M. K. Miller, M. J. Molina, J. Alcamo, J. S. Daniel, D. W. Fahey, S. A. Montzka, S. Reimann, Preserving Montreal Protocol climate benefits by limiting HFCs, *Science* 335 (2012) 922-923.
- [2] T. Jabbour, D. F. Clodic, Burning Velocity and Refrigerant Flammability Classification, *ASHRAE Trans.* 110 (2004) 522-533.
- [3] P. Papas, S. Zhang, W. Kim, S. P. Zeppieri, M. B. Colket, P. Verma, Laminar flame speeds of 2,3,3,3-tetrafluoropropene mixtures, *Proc. Combust. Inst.* 36 (2017) 1145-1154.
- [4] K. Takizawa, N. Igarashi, K. Tokuhashi, S. Kondo, M. Mamiya, H. Nagai, Assessment of Burning Velocity Test Methods for Mildly Flammable Refrigerants, Part 2: Vertical-Tube Method, *ASHRAE Trans.* 119 (2013) 255-264.
- [5] G. T. Linteris, Burning Velocity of 1,1 difluoroethane (R-152a), *ASHRAE Trans.* 112 (2006) 448-458.
- [6] K. Takizawa, A. Takahashi, K. Tokuhashi, S. Kondo, A. Sekiya, Burning velocity measurement of fluorinated compounds by the spherical-vessel method, *Combust. Flame* 141 (2005) 298-307.
- [7] K. Takizawa, A. Takahashi, K. Tokuhashi, S. Kondo, A. Sekiya, Burning velocity measurement of HFC-41, HFC-152a, and HFC-161 by the spherical-vessel method, *J Fluorine Chem* 127 (2006) 1547-1553.
- [8] K. Takizawa, A. Takahashi, K. Tokuhashi, S. Kondo, A. Sekiya, Burning velocity measurements of fluoropropanes by the spherical-vessel method, *J Fluorine Chem* 129 (2008) 713-719.
- [9] K. Takizawa, S. Takagi, K. Tokuhashi, S. Kondo, M. Mamiya, H. Nagai, Assessment of Burning Velocity Test Methods for Mildly Flammable Refrigerants, Part 1: Closed-Vessel Method, *ASHRAE Trans.* 119 (2013) 243-254.
- [10] K. Takizawa, E. Hihara, C. Dang, M. Ito, Fundamental flammability. Burning velocity, in: Risk Assessment of Mildly Flammable Refrigerants. Final Report 2016, The Japan Society of Refrigerating and Air Conditioning Engineers, Tokyo, Japan, 2017, pp. 34-37.
- [11] A. Moghaddas, C. Bennett, E. Rokni, H. Metghalchi, Laminar burning speeds and flame structures of mixtures of difluoromethane (HFC-32) and 1,1-difluoroethane (HFC-152a) with air at elevated temperatures and pressures, *HVAC&R Research* 20 (2014) 42-50.
- [12] R. Burrell, J. L. Pagliaro, G. T. Linteris, Effects of stretch and thermal radiation on difluoromethane-air burning velocity measurements in constant volume spherically expanding flames, *Proc. Combust. Inst.* 37 (2019) 4231-4238.
- [13] M. Hegetschweiler, J. Pagliaro, L. Berger, R. Hesse, J. Beeckmann, H. Pitsch, G. Linteris, Effects of stretch and radiation on the laminar burning velocity of R-32/air flames, *Sci. Technol. Built Environ.* 26 (2020) 599-609.
- [14] R. Hesse, L. Berger, C. Bariki, M. J. Hegetschweiler, G. T. Linteris, H. Pitsch, J. Beeckmann, Low global-warming-potential refrigerant CH₂F₂ (R-32): Integration of a radiation heat loss correction method to accurately determine experimental flame speed metrics, *Proc. Combust. Inst.* 38 (2021) 4665-4672.
- [15] M. J. Hegetschweiler, J. L. Pagliaro, L. Berger, R. Hesse, J. Beeckmann, C. Bariki, H. Pitsch, G. T. Linteris, Data reduction considerations for spherical R-32 (CH₂F₂)-air flame experiments, *Combust. Flame* 237 (2022) 111806.
- [16] Z. Chen, Effects of radiation and compression on propagating spherical flames of methane/air mixtures near the lean flammability limit, *Combust. Flame* 157 (2010) 2267-2276.
- [17] J. Santner, F. M. Haas, Y. Ju, F. L. Dryer, Uncertainties in interpretation of high pressure spherical flame propagation rates due to thermal radiation, *Combust. Flame* 161 (2014) 147-153.
- [18] F. Halter, Z. Chen, G. Dayma, C. Bariki, Y. Wang, P. Dagaut, C. Chauveau, Development of an optically accessible apparatus to characterize the evolution of spherically expanding flames under constant volume conditions, *Combust. Flame* 212 (2020) 165-176.
- [19] A. Movaghar, R. Lawson, F. N. Egolfopoulos, Confined spherically expanding flame method for measuring laminar flame speeds: Revisiting the assumptions and application to C₁C₄ hydrocarbon flames, *Combust. Flame* 212 (2020) 79-92.
- [20] E. F. Fiock, C. F. Marvin, The Measurement of Flame Speeds, *Chemical Reviews* 21 (1937) 367-387.
- [21] D. Bradley, A. Mitcheson, Mathematical solutions for explosions in spherical vessels, *Combust. Flame* 26 (1976) 201-217.
- [22] M. Metghalchi, J. C. Keck, Laminar burning velocity of propane-air mixtures at high temperature and pressure, *Combust. Flame* 38 (1980) 143-154.

- [23] G. A. Lavoie, Correlations of combustion data for SI Engine calculations—laminar flame speed, quench distance and global reaction rates, SAE Transactions (1978) 1015-1033.
- [24] M. Metghalchi, J. C. Keck, Burning velocities of mixtures of air with methanol, isooctane, and indolene at high pressure and temperature, Combust. Flame 48 (1982) 191-210.
- [25] M. Elia, M. Ulinski, M. Metghalchi, Laminar Burning Velocity of Methane–Air–Diluent Mixtures, J. Eng. Gas Turbines Power 123 (2000) 190-196.
- [26] D. Bradley, P. H. Gaskell, X. J. Gu, Burning velocities, Markstein lengths, and flame quenching for spherical methane-air flames: a computational study Combust. Flame 104 (1996) 176-198.
- [27] K. T. Aung, M. I. Hassan, G. M. Faeth, Flame stretch interactions of laminar premixed hydrogen/air flames at normal temperature and pressure, Combust. Flame 109 (1997) 1-24.
- [28] S. Kondo, K. Takizawa, A. Takahashi, K. Tokuhashi, A. Sekiya, Flammability limits of five selected compounds each mixed with HFC-125, Fire Saf. J. 44 (2009) 192-197.
- [29] O. Askari, M. Janbozorgi, R. Greig, A. Moghaddas, H. Metghalchi, Developing alternative approaches to predicting the laminar burning speed of refrigerants using the minimum ignition energy, Sci. Technol. Built Environ. 21 (2015) 220-227.
- [30] A. Omani, L. Tartakovsky, Measurement of the laminar burning velocity using the confined and unconfined spherical flame methods - A comparative analysis, Combust. Flame 168 (2016) 127-137.
- [31] H. Yu, W. Han, J. Santner, X. Gou, C. H. Sohn, Y. Ju, Z. Chen, Radiation-induced uncertainty in laminar flame speed measured from propagating spherical flames, Combust. Flame 161 (2014) 2815-2824.
- [32] M. Faghih, Z. Chen, The constant-volume propagating spherical flame method for laminar flame speed measurement, Science Bulletin 61 (2016) 1296-1310.
- [33] C. Xiouris, T. Ye, J. Jayachandran, F. N. Egolfopoulos, Laminar flame speeds under engine-relevant conditions: Uncertainty quantification and minimization in spherically expanding flame experiments, Combust. Flame 163 (2016) 270-283.
- [34] F. N. Egolfopoulos, N. Hansen, Y. Ju, K. Kohse-Höinghaus, C. K. Law, F. Qi, Advances and challenges in laminar flame experiments and implications for combustion chemistry, Prog. Energy Combust. Sci. 43 (2014) 36-67.
- [35] M. J. Hegetschweiler, G. T. Linteris, Data Reduction Tool for Spherical Constant Volume Flame Experiments, NIST Technical Note 2148, National Institute of Standards and Technology, Gaithersburg, MD, 2021.
- [36] C. C. M. Luijten, E. Doosje, L. P. H. de Goeij, Accurate analytical models for fractional pressure rise in constant volume combustion, International Journal of Thermal Sciences 48 (2009) 1213-1222.
- [37] H. Pitsch, FlameMaster, A C++ Computer Program for 0D Combustion and 1D Laminar Flame Calculations, I. f. T. V. Tech. rep., RWTH Aachen University, may be downloaded from <https://www.itv.rwth-aachen.de/downloads/flamemaster/>, 1998.
- [38] D. R. Burgess, J. A. Manion, R. R. Burrell, V. I. Babushok, M. J. Hegetschweiler, G. T. Linteris, Validated Model for Burning Velocities of R-32/O₂/N₂ Mixtures over a Wide Range of Conditions, in: 11th U. S. National Combustion Meeting, March 24, 2019 - March 27, 2019, Pasadena, CA, United states, The Combustion Institute, Pittsburg, PA, 2019.
- [39] D. R. Burgess, R. R. Burrell, V. I. Babushok, J. A. Manion, M. J. Hegetschweiler, G. T. Linteris, Burning velocities of R-32/O₂/N₂ mixtures: Experimental measurements and development of a validated detailed chemical kinetic model, Combust. Flame 236 (2022) 111795.
- [40] G. Langer, A. Cuoci, L. Cai, U. Burke, C. Olm, H. Curran, T. Turányi, S. Klippenstein, H. Pitsch, Comparing the results and performance of chemical kinetic modeling software, in: 4th International Workshop on Flame Chemistry, Dublin, Ireland, July 28-29, 2018, The Combustion Institute, Pittsburg, PA, 2018.
- [41] G. Langer, A. Cuoci, L. Cai, U. Burke, C. Olm, H. Curran, T. Turányi, H. Pitsch, A Comparison of Numerical Frameworks for Modelling Homogeneous Reactors and Laminar Flames, in: Joint Meeting of the German and Italian Sections of the Combustion Institute, Sorrento, Italy, May 23-26, 2018, The Combustion Institute, Pittsburg, PA, 2018.
- [42] J. L. Pagliaro, Inhibition of laminar premixed flames by Halon 1301 alternatives, Ph.D. Thesis, University of Maryland, College Park, MD, 2015.
- [43] F. A. Williams, A review of some theoretical considerations of turbulent flame structure, in: AGARD Conference Proceeding, AGARD-CP-164, NATO Science and Technology Organization, 1975.
- [44] A. P. Kelley, J. K. Bechtold, C. K. Law, Premixed flame propagation in a confining vessel with weak pressure rise, Journal of Fluid Mechanics 691 (2011) 26-51.
- [45] D. K. Kim, V. I. Babushok, D. R. Burgess, M. J. Hegetschweiler, G. T. Linteris, Burning Velocity of Blends of R-152a with R-134a or R-1234yf and air, Combust. Sci. Technol. (2023) in press.
- [46] Z. Chen, M. P. Burke, Y. Ju, Effects of compression and stretch on the determination of laminar flame speeds using propagating spherical flames, Combust. Theory and Modelling 13 (2009) 343-364.

[47] Z. Chen, Effects of radiation absorption on spherical flame propagation and radiation-induced uncertainty in laminar flame speed measurement, *Proc. Combust. Inst.* 36 (2017) 1129-1136.